

Supporting Information

Coexistence of magnetic ordering and ferroelectricity in a Dy-nitronyl nitroxide chain

Xiaotong Wang,^a Meiyang Liu,^b Yuxia Wang,^a Chaoyi Jin,^a Hongwei Song,^a Zhiliang Liu,^{*b} Jinkui Tang,^{*c} Licun Li^{*a}

^a Department of Chemistry, Key Laboratory of Advanced Energy Materials Chemistry, College of Chemistry, Nankai University, Tianjin 300071, China

^b Inner Mongolia Key Laboratory of Chemistry and Physics of Rare Earth Materials, School of Chemistry and Chemical Engineering, Inner Mongolia University, Hohhot 010021, P.R. China

^c State Key Laboratory of Rare Earth Resource Utilization, Changchun Institute of Applied Chemistry, Chinese Academy of Sciences, Changchun, 130022 China

Table S1. Crystallographic Data and Structure Refinement for **1**

Complex	1
Empirical formula	C ₃₀ H ₂₄ F ₁₈ DyN ₂ O ₉
Mr	1061.01
T, (K)	113
Crystal system	Monoclinic
Space group	P2 ₁
a /Å	22.297(2)
b /Å	16.6711(16)
c /Å	23.000(2)
α /°	90
β /°	116.697(2)
γ /°	90
V /Å ³	7638.0(12)
Z	8
D _{calcd} /g·cm ⁻³	1.845
μ /mm ⁻¹	2.097
θ /°	3.01 to 27.54
F(000)	4144
Reflections collected	98872 / 34384
Unique reflns/R _{int}	0.0249
GOF	1.047
Flack parameter	0.305(7)
R ₁ , wR ₂ (I > 2σ(I))	R ₁ =0.0385, wR ₂ = 0.0964
R ₁ , wR ₂ (all data)	R ₁ =0.0408, wR ₂ = 0.0979

R₁ = Σ(|F_o| - |F_c|)/Σ|F_o|, wR₂ = [Σw(|F_o|² - |F_c|²)²/Σw(|F_o|²)²]^{1/2}

Table S2. Selected bond distances (Å) and angles (°) for complex **1**.

Bond distances			
Dy(1)-O(1)	2.373(6)	Dy(1)-O(2)	2.337(6)
Dy(1)-O(3)	2.317(6)	Dy(1)-O(4)	2.381(7)
Dy(1)-O(5)	2.337(6)	Dy(1)-O(6)	2.332(5)
Dy(1)-O(8)	2.381(6)	Dy(1)-O(9)	2.337(6)
O(8)-N(1)	1.294(8)	O(9)-N(2)	1.300(9)
Dy(2)-O(17)	2.368(5)	Dy(2)-O(10)	2.357(5)
Dy(2)-O(11)	2.333(5)	Dy(2)-O(18)	2.323(5)
Dy(2)-O(14)	2.390(5)	Dy(2)-O(12)	2.318(5)
Dy(2)-O(15)	2.327(5)	Dy(2)-O(13)	2.383(5)

O(17)-N(3)	1.271(8)	O(18)-N(4)	1.296(8)
Dy(3)-O(27)	2.353(5)	Dy(3)-O(23)	2.340(5)
Dy(3)-O(24)	2.360(5)	Dy(3)-O(19)	2.378(5)
Dy(3)-O(20)	2.325(5)	Dy(3)-O(22)	2.330(5)
Dy(3)-O(21)	2.377(5)	Dy(3)-O(26)	2.321(5)
O(27)-N(6)	1.286(8)	O(26)-N(5)	1.275(8)
Dy(4)-O(35)	2.373(5)	Dy(4)-O(32)	2.355(5)
Dy(4)-O(33)	2.324(5)	Dy(4)-O(31)	2.342(5)
Dy(4)-O(28)	2.333(5)	Dy(4)-O(29)	2.357(6)
Dy(4)-O(30)	2.351(5)	Dy(4)-O(36)	2.334(5)
<i>Angles</i>			
O(9)-Dy(1)-O(1)	73.7(2)	O(9)-Dy(1)-O(2)	74.5(2)
O(9)-Dy(1)-O(3)	101.7(2)	O(9)-Dy(1)-O(4)	73.1(2)
O(9)-Dy(1)-O(5)	145.3(2)	O(9)-Dy(1)-O(6)	86.1(2)
O(9)-Dy(1)-O(8)	142.1(2)	O(8)-Dy(1)-O(1)	71.11(2)
O(2)-Dy(1)-O(8)	82.0(2)	O(3)-Dy(1)-O(8)	84.7(2)
O(8)-Dy(1)-O(4)	142.5(2)	O(5)-Dy(1)-O(8)	72.6(2)
O(6)-Dy(1)-O(8)	112.9(2)	N(2)-O(9)-Dy(1)	153.3(6)
N(1)-O(8)-Dy(1)	138.6(5)	O(18)-Dy(2)-O(17)	140.09(17)
O(18)-Dy(2)-O(10)	74.56(18)	O(18)-Dy(2)-O(11)	73.14(19)
O(18)-Dy(2)-O(14)	145.51(17)	O(18)-Dy(2)-O(15)	97.15(18)
O(18)-Dy(2)-O(13)	71.12(18)	O(12)-Dy(2)-O(17)	94.05(17)
O(10)-Dy(2)-O(17)	70.63(18)	O(11)-Dy(2)-O(17)	78.78(18)
O(15)-Dy(2)-O(17)	101.28(18)	N(4)-O(18)-Dy(2)	145.8(4)
N(3)-O(17)-Dy(2)	134.6(4)	O(27)-Dy(3)-O(24)	75.50(18)
O(27)-Dy(3)-O(21)	69.34(17)	O(23)-Dy(3)-O(24)	72.88(18)
O(23)-Dy(3)-O(21)	144.59(18)	O(20)-Dy(3)-O(27)	92.82(19)
O(20)-Dy(3)-O(23)	140.26(19)	O(20)-Dy(3)-O(19)	72.79(19)
O(22)-Dy(3)-O(23)	70.90(18)	O(22)-Dy(3)-O(24)	126.0(2)
O(21)-Dy(3)-O(19)	129.71(19)	O(26)-Dy(3)-O(23)	93.1(2)
N(6)-O(27)-Dy(3)	134.7(5)	N(5)-O(26)-Dy(3)	150.0(5)
O(32)-Dy(4)-O(35)	71.13(18)	O(32)-Dy(4)-O(29)	133.38(18)
O(33)-Dy(4)-O(32)	74.15(18)	O(33)-Dy(4)-O(30)	131.16(19)
O(33)-Dy(4)-O(36)	73.1(2)	O(31)-Dy(4)-O(35)	91.77(17)
O(31)-Dy(4)-O(29)	76.90(19)	O(28)-Dy(4)-O(35)	104.23(18)
O(28)-Dy(4)-O(29)	72.71(19)	O(30)-Dy(4)-O(32)	126.57(19)
N(7)-O(35)-Dy(4)	134.3(4)	N(8)-O(36)-Dy(4)	154.2(5)

Table S3. SHAPE analysis for the complex **1**.

Complex	SAPR-8	TDD-8	JBTPR-8	BTPR-8	JSD-8
Dy1	1.158	1.055	1.854	1.289	3.581
Dy2	2.810	0.117	3.000	2.378	2.780
Dy3	2.045	0.211	2.407	1.857	2.877
Dy4	1.594	0.260	2.582	1.939	3.123

(SAPR-8: square antiprism. TDD-8: triangular dodecahedron. JBTPR-8: biaugmented trigonal prism J50. BTPR-8: biaugmented trigonal prism. JSD-8: snub diphenoid J84.)

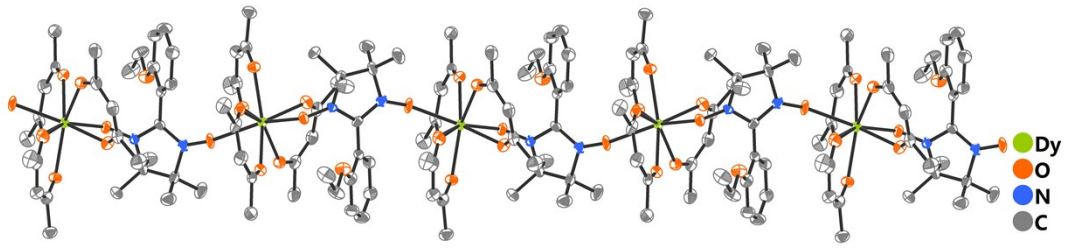


Figure S1. The ORTEP-style diagram of complex **1** with thermal ellipsoids at 30% probability, H and F atoms are not shown for the sake of clarity.

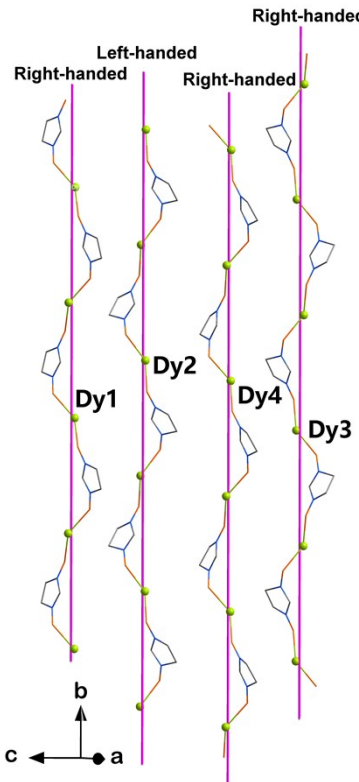


Figure S2. Four helical chains in the crystal lattice along the *b* axis (Some atoms are omitted for clarity).

Figure S3. Coordination polyhedrons of the Dy^{III} ions in complex **1**.

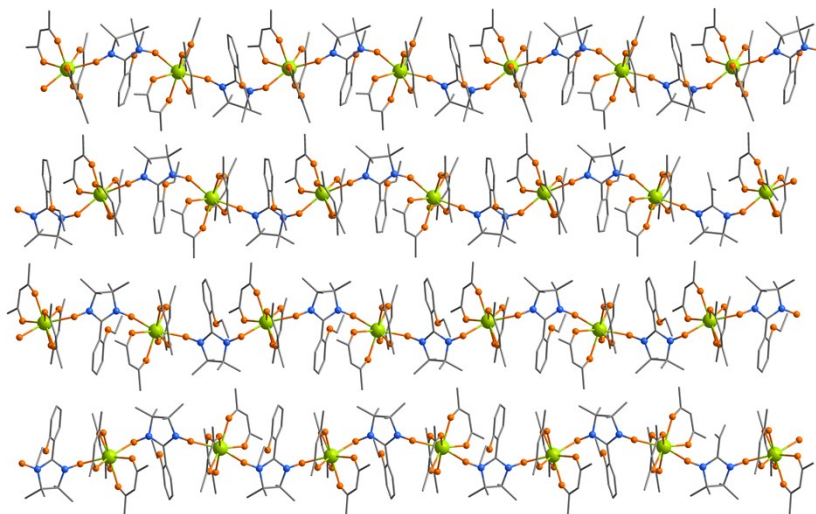


Figure S4. Packing diagram of complex **1**, H and F atoms are not shown for the sake of clarity.

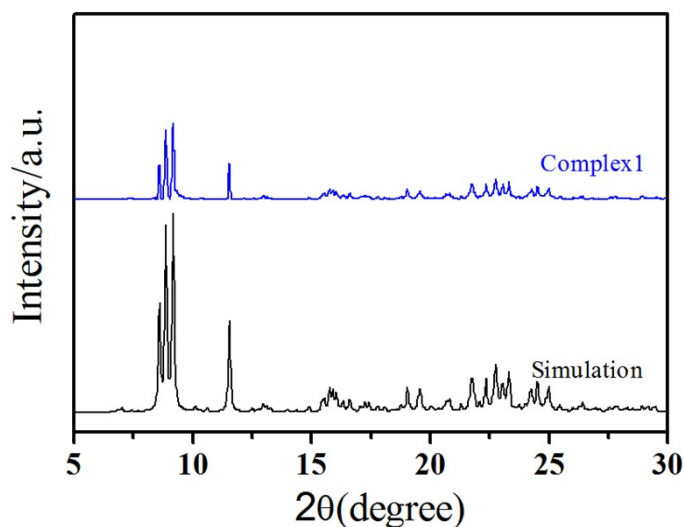


Figure S5. Powder X-ray diffraction patterns (PXRD) of **1**.

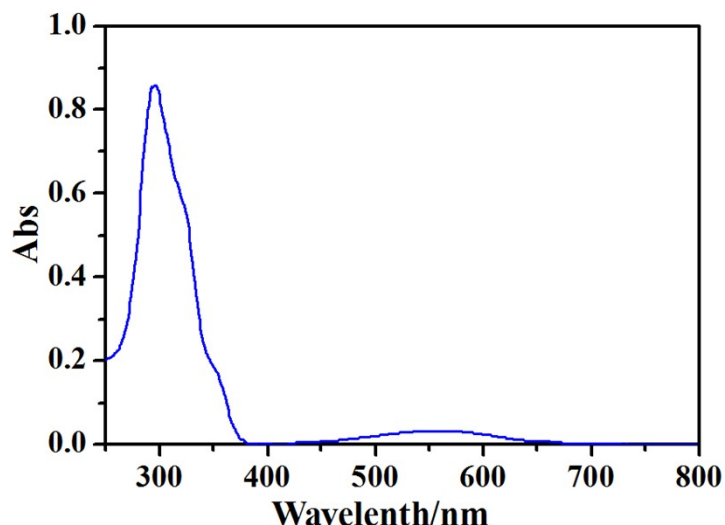


Figure S6. UV-vis spectra of complex **1** (1.0×10^{-5} M in CH_2Cl_2)

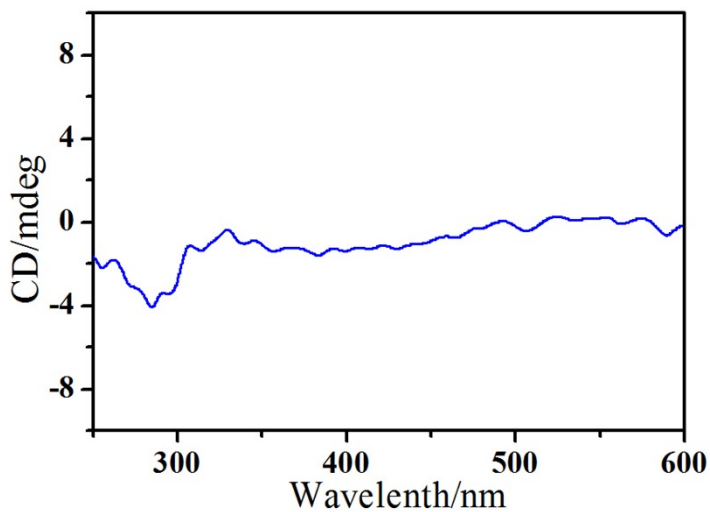


Figure S7. CD spectra of complex **1** in KBr pellet.

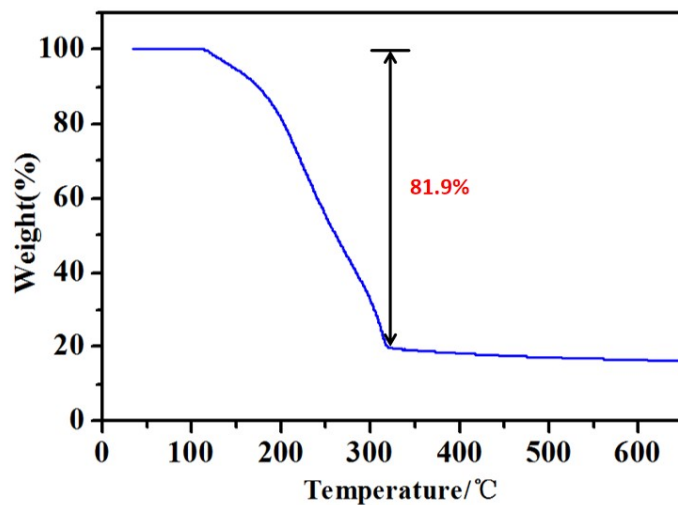


Figure S8. The TGA curve of complex **1**.

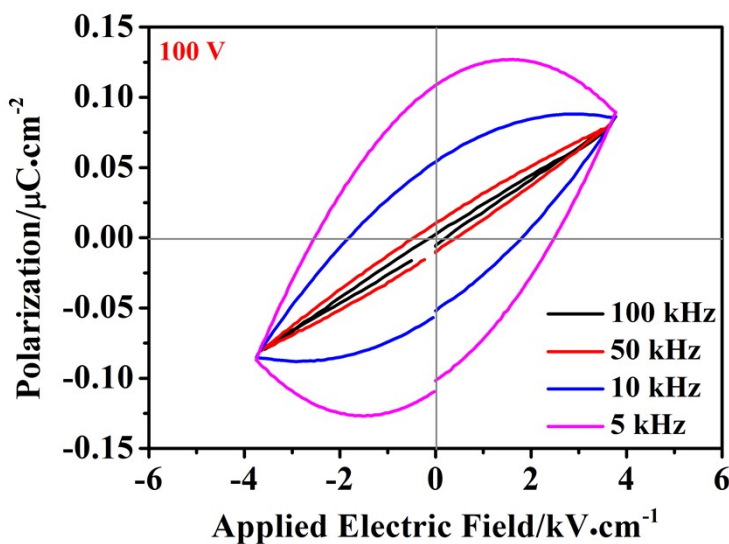


Figure S9. Frequency-dependent *P-E* hysteresis loops of complex **1**.

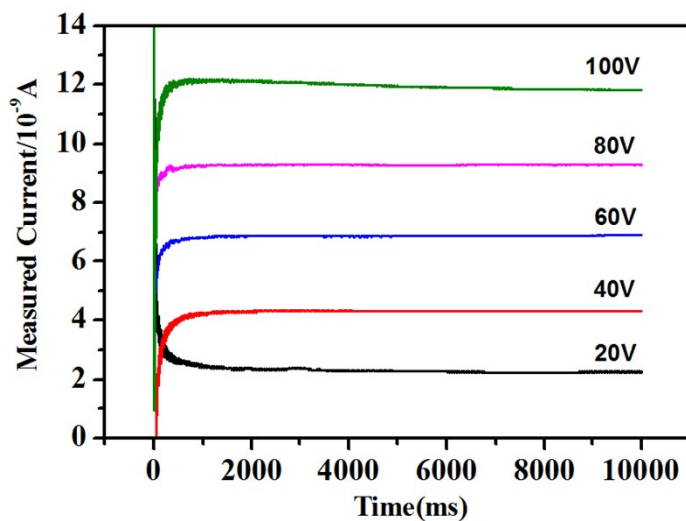


Figure S10. The leakage current of complex 1 when the voltage ranges from 20-100 V.

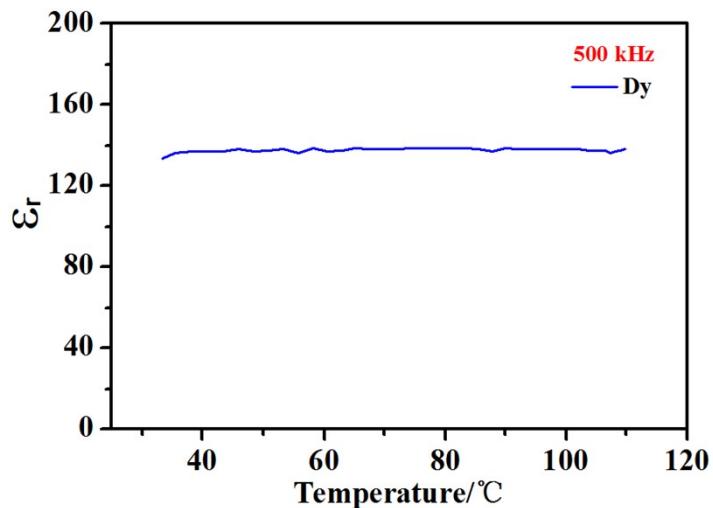


Figure S11. The dielectric constant of complex 1 at 500 kHz in the temperature range of 30-110 °C.

Figure S12. The DSC curves of complex 1.

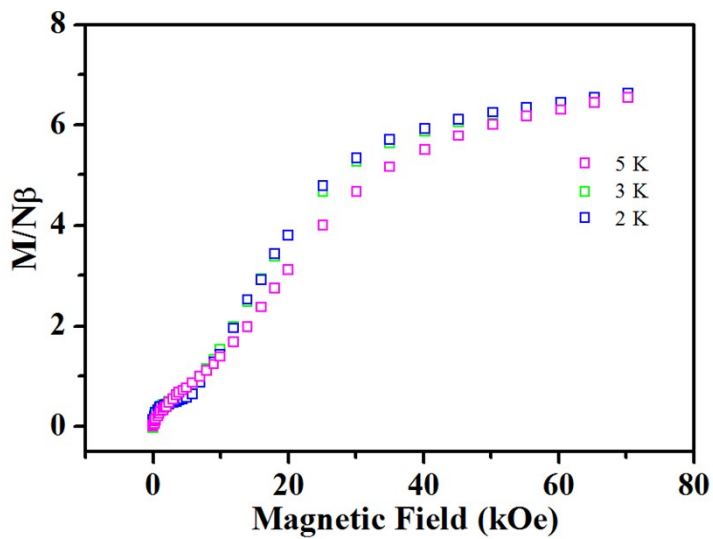


Figure S13. M vs H plots of **1** at 2-5 K.

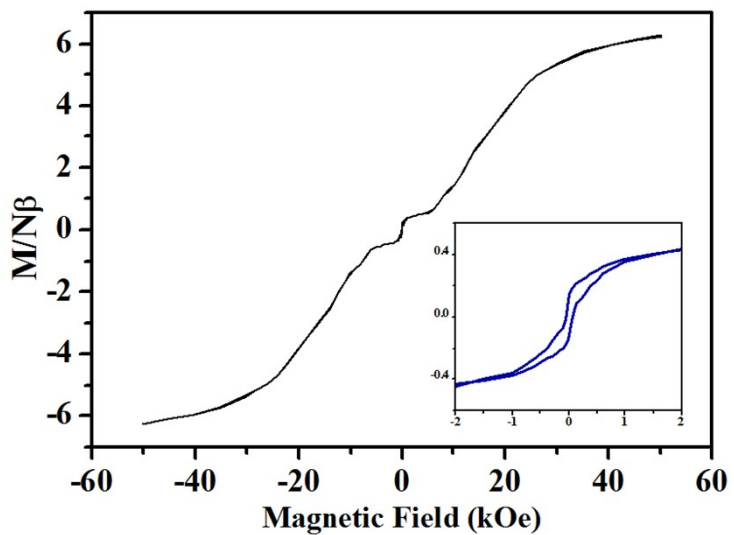


Figure S14. The hysteresis loop plot of **1** at 2 K.

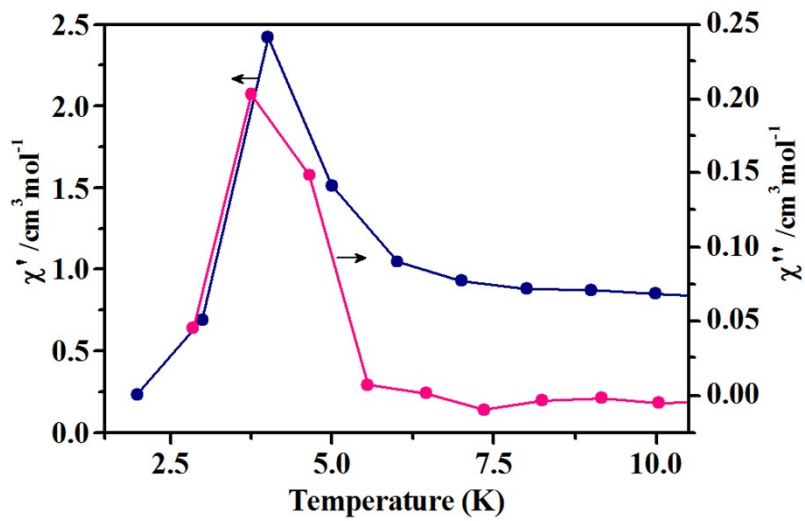


Figure S15. Measured χ' and χ'' versus T plots under 170 dc field at the frequency of 997 Hz.

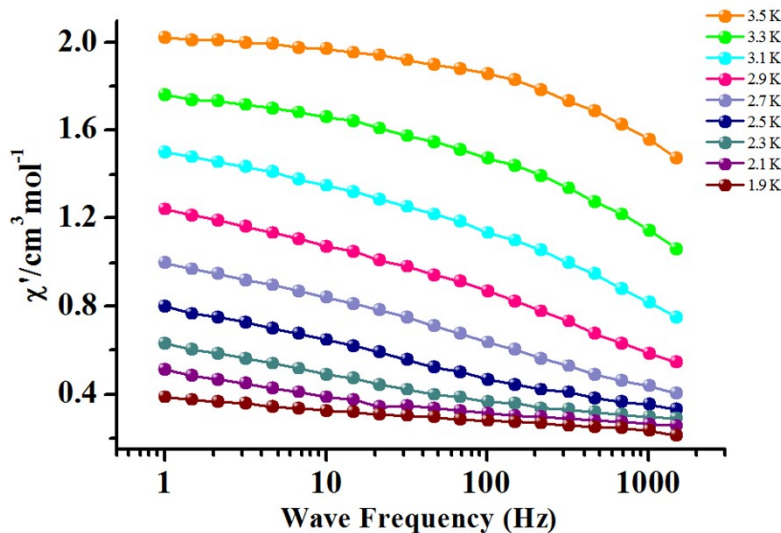


Figure S16. Frequency dependence of χ'_{ac} susceptibility under 170 Oe dc field for **1**.

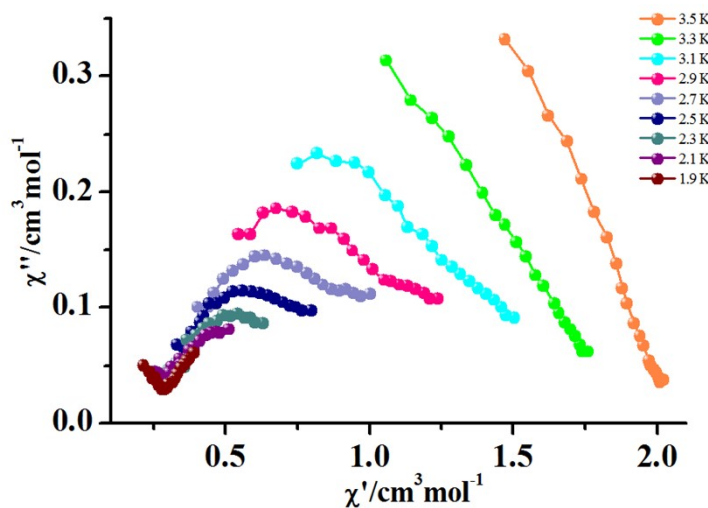


Figure S17. Cole–Cole plots for **1**.